

Neutrino Clustering in Cold Dark Matter Halos : Implications for Ultra High Energy Cosmic Rays

Shwetabh Singh* and Chung-Pei Ma†

*Department of Astronomy,
University of California at Berkeley,
601 Campbell Hall, Berkeley, CA 94720*

We develop a method based on the collisionless Boltzmann equation to calculate the gravitational clustering of relic neutrinos in realistic cosmological models dominated by cold dark matter (CDM) and the cosmological constant. This method can be used to estimate the phase-space distribution of any light particles in CDM halos. We find that neutrinos with masses $\gtrsim 0.3$ eV cluster appreciably in dark matter halos above the galactic size. The resulting neutrino overdensity above the cosmic mean neutrino density, δ_ν , increases with both the neutrino mass and the halo mass, ranging from $\delta_\nu \sim 10$ for 0.3 eV neutrinos in $\sim 10^{13} M_\odot$ halos to $\delta_\nu \sim 1500$ for 1.8 eV neutrinos in $\sim 10^{15} M_\odot$ halos. We examine the implications of neutrino clustering for the Z-burst model of ultra high energy cosmic rays (UHECR), which interprets the observed events at $E > 4 \times 10^{19}$ eV as decay products of Z-bosons from the resonant scattering between relic and high energy neutrinos and anti-neutrinos. We estimate the UHECR energy spectrum for various neutrino masses towards five of the most massive clusters in the local universe (within 100 Mpc): Virgo, Perseus-Pisces, Hydra, Centaurus, and Coma. The UHECR flux in the Z-burst model is expected to be significantly higher towards these clusters if $m_\nu \gtrsim 0.3$ eV and nearly isotropic otherwise.

I. INTRODUCTION

The nature of cosmic rays above the Greisen-Zatsepin-Kuzmin (GZK) cutoff [1] at $\sim 4 \times 10^{19}$ eV is an unsolved problem in ultra high energy cosmic ray (UHECR) physics [2]. These events have been reported by the AGASA [3], Fly's Eye [4], Haverá Park [5], HiRes [6], and Yakutsk [7] collaborations. Photoproduction of pions ($p\gamma_{BRR} \rightarrow p+N\pi, n\gamma_{BRR} \rightarrow n+N\pi$), photopair production ($p\gamma_{BRR} \rightarrow pe^+e^-, \gamma\gamma_{BRR} \rightarrow e^+e^-$), and inverse Compton scattering ($e^\pm\gamma_{BRR} \rightarrow e^\pm\gamma, p\gamma_{BRR} \rightarrow p\gamma$) at high energies [8] constrain a $\sim 10^{20}$ eV cosmic ray to a few Mpc for the characteristic lengths of either charged cosmic rays or neutrons and photons. More specifically, the attenuation length of protons above the GZK cutoff is ~ 50 Mpc, which would require novel powerful acceleration mechanisms for light nuclei in nearby galaxies [9]. The lack of known processes to accelerate cosmic rays in small galactic objects makes the galactic origin of these ultra high energy particles unfeasible [10]. Attempts to circumvent the problems of conventional primaries and interactions have been made by the introduction of exotic particles and dynamics, but these come with their own difficulties [2].

One proposed explanation for the UHECRs is the Z-burst model, which tries to solve the puzzle without invoking new physics beyond the standard model of particle physics except for neutrino masses. Several recent experiments [11, 12, 13] have found evidence for non-zero neutrino mass. The Z-burst model hinges on the

fact that ultra high energy neutrinos (and anti-neutrinos) produced at cosmological distances can reach the GZK zone ($\lesssim 100$ Mpc) unattenuated. Their resonant annihilation on the relic anti-neutrinos (and neutrinos) produces Z bosons, about 70% of which decay into hadrons within $\sim 10^{-25}$ sec. The final state has fifteen pions and 1.35 baryon-antibaryon pairs on average [14], where the fifteen pions decay into thirty high energy photons. The Z boson is highly boosted ($\sim 10^{10}$) [15], resulting in a highly collimated beam with a half angle of $\sim 10^{-10}$. This and the fact that the effect of magnetic fields at such high energies is negligible [16] ensure a high probability for the protons and photons to reach the observer if the Z-burst occurs in the direction of the Earth. The Z-burst model has been discussed in detail in many papers [17, 18, 19, 20, 21, 22, 23]. The resulting cosmic ray flux has been shown to depend strongly on the density of the relic neutrinos [14, 15, 19], but the neutrino density in these calculations has been taken to be either the constant relic density from the big bang or some ad hoc value.

In this paper we perform a detailed calculation of the neutrino clustering in the local universe using realistic cosmological models and apply the results to the Z-burst model for UHECRs. Since the current constraints from cosmological observations and laboratory experiments indicate that the neutrino masses are small ($\lesssim 2$ eV; see Sec II) and the CDM dominates the dark matter density ($\Omega_{\text{cdm}} \gg \Omega_\nu$), we do not expect the clustering of neutrinos to affect significantly that of the CDM. As a result, it is not essential to use full scale, time consuming N -body simulations. Instead, we solve the collisionless Boltzmann equation for the neutrino phase space distribution in a background potential given by the universal profile of CDM halos reported in recent high resolution

*shwetabh@astro.berkeley.edu

†cpma@astro.berkeley.edu

simulations [24]. The Boltzmann equation is then linear in the neutrino density contrast and has tractable integral solutions. The advantage of this method over the conventional N -body simulations is that we can obtain the neutrino density profile much below the resolution scale of large cosmological simulations (~ 50 kpc) by using as an input the CDM potential determined from much higher resolution simulations of individual halos. Moreover, the computation time required for our approach is negligible compared with numerical simulations, thereby allowing us to explore a large parameter space of neutrino masses and dark matter halo masses.

In Sec II the relevant Boltzmann equation and the integral solutions are derived. In Sec III results for the clustering of neutrinos for different neutrino masses and CDM halos are presented and compared with physical arguments based on neutrino free streaming and the Tremaine-Gunn constraint [27]. The resulting neutrino density profiles are also compared with earlier N -body simulations [28], which show good agreement. In Sec IV the neutrino overdensity calculation is incorporated in the Z-burst model for UHECRs, where we make realistic predictions for the UHECR energy spectrum for different neutrino masses. We estimate the level of anisotropy in the UHECR flux by examining lines of sight towards five of the most massive clusters (Virgo, Perseus-Pisces, Hydra, Centaurus, and Coma) in the local universe (within 100 Mpc) where the neutrinos are likely to be most clustered.

II. BOLTZMANN EQUATION FOR NEUTRINO CLUSTERING IN CDM HALOS

In this section we develop an approach based on the collisionless Boltzmann equation to study how massive neutrinos cluster gravitationally in realistic cosmological models. We start by noting that the median velocity of unclustered background neutrinos of mass m_ν (in eV) at redshift z is

$$\bar{v} = 161(1+z)m_\nu^{-1} \text{ km s}^{-1}. \quad (1)$$

This implies that light neutrinos ($m_\nu \lesssim 2$ eV) do not accrete significantly onto CDM protoclusters until $z \sim 4$ because the neutrino thermal velocities are greater than the velocity dispersion of a typical cluster or supercluster. We are then faced with the more tractable problem of how neutrinos cluster in the potential well of an existing CDM halo. Our approach is to use the collisionless Boltzmann equation for the neutrino phase space density f and follow its evolution in a background CDM potential given by the approximate universal profile obtained in high resolution simulations of individual halos [24]. Earlier work has used the Boltzmann approach to study how neutrinos cluster around point masses in the context of cosmic string seeded galaxy formation [25, 26]. This method allows us to calculate the neutrino density profiles in the inner part of the cluster ($\lesssim 10$ kpc) that can

not be resolved by large cosmological simulations. This will be seen to be important in the Z-burst model where a significant contribution to the cosmic ray flux comes from the core of the halo.

In the Newtonian approximation and in physical coordinates, the collisionless Boltzmann equation takes the form

$$\frac{\partial f}{\partial t} + \dot{\mathbf{r}} \cdot \nabla_{\mathbf{r}} f + \dot{\mathbf{p}} \cdot \nabla_{\mathbf{p}} f = 0. \quad (2)$$

Rewriting it in conformal time $d\tau = dt/a$ and in comoving position $\mathbf{x} = \mathbf{r}/a$ and momentum $\mathbf{q} = a\mathbf{p} - m_\nu \dot{a}\mathbf{r}$, we obtain

$$\begin{aligned} \frac{1}{a} \frac{\partial f}{\partial \tau} + \frac{\mathbf{q}}{m_\nu a^2} \cdot \nabla_{\mathbf{x}} f - m_\nu \ddot{a} \mathbf{x} \cdot \nabla_{\mathbf{q}} f \\ - m_\nu \nabla_{\mathbf{x}} \Phi \cdot \nabla_{\mathbf{q}} f = 0. \end{aligned} \quad (3)$$

where the Newtonian gravitational potential Φ obeys $\dot{\mathbf{p}} = -m_\nu \nabla \Phi$. At the time of decoupling the neutrino phase space density is given by the thermal Fermi-Dirac distribution $f_0(q) \propto (e^{q/T_{\nu,0}} + 1)^{-1}$ where $T_{\nu,0} = (4/11)^{1/3} T_{\gamma,0} = 1.637 \times 10^{-4}$ eV is the temperature of the neutrino background today. Gravitational clustering distorts the spatially uniform f_0 , so we write the full distribution as

$$f(\mathbf{x}, \mathbf{q}, \tau) = f_0(q) + f_1(\mathbf{x}, \mathbf{q}, \tau). \quad (4)$$

The gravitational potential can also be written as

$$\Phi(\mathbf{x}, \tau) = \Phi_0(\mathbf{x}, \tau) + \Phi_1(\mathbf{x}, \tau) \quad (5)$$

where Φ_0 is related to the mean background comoving density $\bar{\rho} = \bar{\rho}_{\text{cdm}} + \bar{\rho}_\nu$ by $\nabla_{\mathbf{x}} \Phi_0 = \frac{4\pi}{3} G \bar{\rho} a^2 \mathbf{x}$, and Φ_1 is determined by the density contrast of both CDM and neutrinos in the halo:

$$\begin{aligned} \nabla_{\mathbf{x}}^2 \Phi_1 &= 4\pi G a^2 (\delta\rho_{\text{cdm}} + \delta\rho_\nu) \\ &= 4\pi G a^2 \bar{\rho} (\Omega_{\text{cdm}} \delta_{\text{cdm}} + \Omega_\nu \delta_\nu). \end{aligned} \quad (6)$$

Equation (3) then becomes

$$\begin{aligned} \frac{1}{a} \frac{\partial f_1}{\partial \tau} + \frac{\mathbf{q}}{m_\nu a^2} \cdot \nabla_{\mathbf{x}} f_1 - m_\nu \nabla_{\mathbf{x}} \Phi_1 \cdot \nabla_{\mathbf{q}} f_0 \\ - m_\nu \nabla_{\mathbf{x}} \Phi_1 \cdot \nabla_{\mathbf{q}} f_1 = 0. \end{aligned} \quad (7)$$

We note that this is the full Boltzmann equation and no approximation has been made thus far. It is generally a nonlinear equation in f_1 where Φ_1 is related to f_1 . For our problem, however, Φ_1 is mostly determined by the CDM whose potential has a well known, pre-determined form. Equation (7) is then linear in f_1 and much easier to solve.

Furthermore, equation (7) has a simple integral solution if the fourth term is neglected. For example, in earlier calculations that examined neutrino clustering onto point masses seeded by cosmic strings, this term was dropped in order to simplify the calculation [25, 26]. We

will also proceed by ignoring this term, but we justify this approach in two ways. First, we note that the dropping of this term requires $\nabla_q f_1 < \nabla_q f_0$ and not $f_1 < f_0$. The former is generally a less restrictive condition and can be satisfied even when f_1 is much larger than f_0 because on dimensional grounds, we have

$$\frac{\nabla_q f_1}{\nabla_q f_0} \sim \frac{f_1/\sigma_v}{f_0/\bar{v}} \sim \frac{\delta\rho_\nu/\sigma_v^4}{\rho_\nu/\bar{v}^4} \sim \delta_\nu \left(\frac{\bar{v}}{\sigma_v} \right)^4, \quad (8)$$

where σ_v is the velocity dispersion of the gravitational potential Φ_1 and \bar{v} is the median neutrino thermal velocity in equation (1). Since only neutrinos with $\bar{v} \ll \sigma_v$ are cold enough to fall into the gravitational wells, we expect the ratio $\nabla_q f_1/\nabla_q f_0$ to be much smaller than f_1/f_0 , thereby making it easier to justify the dropping of the fourth term in equation (7). Equation (8) further indicates that δ_ν is larger than f_1/f_0 by $(\sigma_v/\bar{v})^3$, a large factor in highly clustered regions. This explains qualitatively the large δ_ν found in our numerical results to be presented in Sec III. In the next section we also provide further justification for ignoring the $\nabla_q f_1$ term by comparing our results with the neutrino density profiles of two halos obtained from earlier numerical simulations.

Following [25], we convert equation (7) into an ordinary differential equation by going into Fourier space and using a new time variable $d\eta = d\tau/a$:

$$\frac{\partial \tilde{f}_1}{\partial \eta} + \frac{i\mathbf{k} \cdot \mathbf{q}}{m_\nu} \tilde{f}_1 + \frac{im_\nu}{k^2} 4\pi G a^4 \tilde{\rho} \mathbf{k} \cdot \nabla_q f_0 = 0, \quad (9)$$

where \tilde{f}_1 and $\tilde{\rho}$ are the Fourier transforms of f_1 and ρ . The solution is

$$\begin{aligned} \tilde{f}_1(\mathbf{k}, \mathbf{q}, \eta) = & -\frac{im_\nu}{k^2} 4\pi G \int_{\eta_0}^{\eta} d\eta' e^{-i\mathbf{k} \cdot \mathbf{q}(\eta - \eta')/m_\nu} \\ & \times a^4(\eta') \tilde{\rho}(\mathbf{k}, \eta') \mathbf{k} \cdot \nabla_q f_0, \end{aligned} \quad (10)$$

where we have taken the initial neutrino phase space to be homogeneous, i.e., $f_1(\eta_0) = 0$ and $f(\eta_0) = f_0$.

The neutrino overdensity is given by

$$\tilde{\delta}_\nu(\mathbf{k}, \eta) = \frac{m_\nu}{\bar{\rho}_\nu h_p^3} \int d^3\mathbf{q} \tilde{f}_1(\mathbf{k}, \mathbf{q}, \eta), \quad (11)$$

which can be obtained from equation (10) after integration by parts in \mathbf{q} and integration over angles:

$$\begin{aligned} \tilde{\delta}_\nu(k, \eta) = & \frac{16\pi^2 G m_\nu^2}{\bar{\rho}_\nu h_p^3 k} \int_{\eta_0}^{\eta} d\eta' a^4(\eta') \tilde{\rho}(k, \eta') \\ & \times \int_0^\infty dq q \frac{\sin[k q(\eta - \eta')/m_\nu]}{e^{q/T_{\nu,0}} + 1} \end{aligned} \quad (12)$$

where $\bar{\rho}_\nu = m_\nu \bar{n}_\nu$ is the mean comoving mass density of neutrinos and $\bar{n}_\nu \approx 54 \text{ cm}^{-3}$ per species of light neutrinos, and h_p is the Planck constant. Equation (12) is the main equation that we will solve in this paper. It is a Volterra integral equation of the second kind that has

the form $f(t) = \int_a^t ds K(t, s)f(s) + g(t)$ and can be solved with the trapezoidal rule. It describes how neutrinos of a given mass m_ν cluster around a realistic CDM halo of density profile ρ_{cdm} as a function of time. The density of the cluster at a given time, $\tilde{\rho}$, is the sum of the both the CDM and the neutrino components.

III. RESULTS FOR NEUTRINO CLUSTERING IN CDM HALOS

In this section we present results for δ_ν computed from equation (12). We choose to integrate equation (12) from $z = 3$ to 0; the results differ by only about 5% if the initial redshift is pushed back to 5 because the neutrinos do not cluster appreciably at such early times as discussed above. We also need to specify the cosmological models and neutrino masses. For the cosmological parameters, we use the currently favored critically-flat model with matter density $\Omega_m = \Omega_{\text{cdm}} + \Omega_\nu = 0.35$, cosmological constant $\Omega_\Lambda = 0.65$, and Hubble constant $h = 0.7$. Variations in these parameters at 10 to 20% level are not expected to alter our neutrino results significantly since the effect on the halo potential Φ_1 is small. For the neutrino masses, we consider four different models in which three models assume one massive species with masses 1.8, 0.7, and 0.2 eV respectively, and one model with two massive species with masses 0.4 and 0.3 eV. The corresponding density parameter in neutrinos is $\Omega_\nu \approx 0.04, 0.015, 0.004$ and 0.015, respectively, all much smaller than Ω_{cdm} . This range of neutrino masses is chosen to span the current cosmological and laboratory limits. The most recent cosmological constraint comes from the galaxy clustering power spectrum of the 2dF (2 Degree Field) redshift survey, which places an upper limit of 1.8 eV on the sum of the neutrino masses [29]. The Super-Kamiokande experiment [11] provides strong evidence for oscillations between neutrino species with a mass difference of $\delta m^2 = (1 - 8) \times 10^{-3} \text{ eV}$, giving a minimum mass of 0.07 eV if the neutrino masses are hierarchical.

Although the final neutrino density profile will depend strongly on the CDM profile, we do not expect the reverse to hold: CDM density will not be much affected by the clustering of neutrinos because all the models considered in this paper have small $\Omega_\nu/\Omega_{\text{cdm}}$, so the CDM dominates the gravitational potential of a dark matter halo. We are therefore justified in using the universal CDM profile determined from the high resolution pure CDM simulations [24] as the input:

$$\rho_{\text{cdm}}(r) = \frac{\bar{\rho} \bar{\delta} r_s^3}{r(r + r_s)^2}, \quad (13)$$

where $\bar{\delta}$ and r_s are given in terms of the concentration parameter [30, 31]

$$c = \frac{9}{1+z} \left(\frac{M}{1.5 \times 10^{13} h^{-1} M_\odot} \right)^{-0.13},$$

$$\bar{\delta} = \frac{200c^3}{3[\ln(1+c) - c/(1+c)]}, \quad (14)$$

$$r_s = \frac{1.63 \times 10^{-5}}{\Omega_m^{1/3} c} \left(\frac{M}{h^{-1} M_\odot} \right)^{1/3} h^{-1} \text{Mpc}.$$

We evaluate the mass density ρ on the right hand side of equation (12) exactly by adding the CDM density given above and the neutrino density computed from previous time steps. We did find that approximating ρ with the CDM profile alone (i.e. ignoring the neutrino contribution to the total potential) changes our results by no more than 10% for the light neutrino masses and cosmological parameters considered in this paper. We also tested the simplifying assumption made in [25], which allowed them to reduce the integrals in equation (12) analytically to a single integral by using $(e^{q/T_{\nu,0}} + 1)^{-1} = A e^{-q/T_{\nu,0}}$, i.e., by assuming a Maxwell-Boltzmann instead of Fermi-Dirac distribution. We found this simplification to cause a $\sim 20\%$ difference at small scales, so we do not use this approximation here.

Before presenting our results for the realistic models above, we first conduct a comparison study by checking our results for the neutrino density profile against those in the numerical simulations of Ref. [28], which investigated the clustering of CDM and neutrinos in two flat cosmological models: $\Omega_{\text{cdm}} = 0.8$ and $\Omega_\nu = 0.2$ with two species of 2.3 eV neutrinos, and $\Omega_{\text{cdm}} = 0.7$ and $\Omega_\nu = 0.3$ with one species of 7 eV neutrinos. Both models assumed $h = 0.5$. These models are no longer consistent with current observations, but the simulation results provide a useful tool for us to test the validity of our Boltzmann approach. For a fair comparison, we use the CDM halo profile found in [28] as an input:

$$\rho_{\text{cdm}}(r) = \frac{C}{r(r+R)^\alpha}, \quad (15)$$

where R and α are 0.3 Mpc and 1.5 for the $\Omega_\nu = 0.2$ model and 0.11 Mpc and 1.1 for the $\Omega_\nu = 0.3$ model. We note that their outer profile is shallower than equation (13) from the pure CDM simulations [24]. In Ref. [28] this difference was attributed to the differing spectral index n for the matter power spectrum of the neutrino models at the mass scale of the simulated halos ($\approx 1.3 \times 10^{15} M_\odot$): $n \simeq -1.36$ for $\Omega_\nu=0.2$ and $n \simeq -1.53$ for $\Omega_\nu=0.3$. This argument, however, appears to be inconsistent with the near universal nature of the halo density profile reported in Ref. [24]. A better understanding for the origin of halo profiles should help resolve this issue.

Figure 1 compares the ratio of the neutrino and CDM density profiles from our approach vs. the two simulated halos in Ref. [28]. For both halos we have used the same cosmological parameters, CDM profiles, and halo mass in our Boltzmann approach as in their simulations. We find a good agreement between the two methods for the outer parts of the cluster; whereas our results are lower by about 50% in the inner parts. This discrepancy may be

due to our neglecting the fourth term in equation (7), or due to statistical fluctuations in the substructure in their simulations. (Unfortunately only two simulated halos are presented in Ref. [28].) The Boltzmann approach used here also allows us to explore how neutrinos respond to different CDM potentials. As an illustration of this, we show in Figure 1 how the neutrino profile changes when the input CDM profile is changed from equation (15) to the higher resolution profile of equation (13). We conclude from Figure 1 that we can obtain a reasonable estimate for neutrino clustering using equation (12) instead of full scale N -body simulations.

We now turn to our results for the realistic cosmological models and neutrino masses given at the beginning of this section. The four panels in Figure 2 show the neutrino overdensity $\delta_\nu = \rho_\nu/\bar{\rho}_\nu - 1$ computed from equation (12) for four different sets of neutrino masses. The more massive neutrinos clearly cluster more because of their lower thermal velocities. Within each panel, the four curves illustrate how δ_ν increases with increasing halo masses from 10^{12} to $10^{15} M_\odot$ as a result of the deeper halo gravitational potentials. The growth of δ_ν in the inner parts of the halo is illustrated in Figure 3 for 0.7 and 0.4 eV neutrinos in 10^{15} , 10^{14} , and $10^{13} M_\odot$ halos. Most of the clustering is seen to occur at low redshifts.

Unlike the CDM density that continues to rise towards the inner part of a halo as $\rho \propto 1/r$, all curves in Figure 2 show that δ_ν flattens out at some radius. Similar features were also seen in Ref. [26] for neutrinos clustered around cosmic strings. This relative suppression in the neutrino vs. CDM overdensity reflects neutrino free streaming, which dampens and retards perturbation growth on small length scales due to phase mixing. This neutrino damping scale, R_d , can be characterized by the length scale above which neutrinos behave like the CDM and the Boltzmann hierarchy can be truncated beyond the $l = 1$ Legendre mode as is done for CDM [32]. Below R_d , more l -modes must be included to compute the neutrino damping effect accurately. This scale is given by [32]

$$R_d(\tau) \equiv \frac{\tau}{\sqrt{1 + [a(\tau)/a_{nr}]^2}}, \quad (16)$$

where $a_{nr} \simeq 3T_{\nu,0}/m_\nu$ is the expansion factor at which the neutrinos become non-relativistic. For the cosmological models considered in this paper, it gives $R_d(z=0) \approx 5.8/m_\nu(\text{eV})$ Mpc. As shown in Figure 1, we indeed find $\rho_\nu/\rho_{\text{cdm}}$ to be about the cosmic mean value $\Omega_\nu/\Omega_{\text{cdm}}$ at scales above R_d and to decrease gradually at smaller radii (top panels), with a final flattening in δ_ν at $r \sim 0.1 R_d$ (bottom panels). Figure 2 shows that the radius at which δ_ν flattens out depends weakly on the mass of the CDM halo. It occurs at smaller radii for less massive CDM halos primarily because the lower mass halos provide shallower potential wells. The damping scale R_d of equation (16) is to be contrasted with the neutrino free streaming distance, which is typically defined as the comoving distance traversed from the time of neutrino

decoupling to a_{nr} : $\lambda_{fs} \equiv \int_{\tau_i}^{\tau_{nr}} d\tau'/a(\tau') \simeq 600/m_\nu(\text{eV})$ Mpc [33]. The distance λ_{fs} reflects the global streaming motion of neutrinos but not the local clustering properties of neutrinos around CDM after they become non-relativistic.

Another way to understand the results in Figures 1 and 2 is to compare the thermal velocities of neutrinos with the velocity dispersions of the CDM halos: neutrinos can cluster significantly only if their mean thermal velocity in equation (1) is below the typical velocity of the host CDM halo. Figure 4 compares these two characteristic velocities for a range of neutrino masses and halo masses. Since the NFW profile specifies only the spatial and not the velocity distribution of the CDM halo particles, two velocity ellipsoids are shown for comparison: isotropic, which is appropriate near the center of the halo, and the more radial distribution $\beta = 1 - v_t^2/v_r^2 = 0.5$, which is appropriate for the outer regions. Figure 4 illustrates that < 0.2 eV neutrinos are too hot to be captured significantly by $\lesssim 10^{14}M_\odot$ halos, while the more massive neutrinos can fall into progressively higher mass halos, a result consistent with that shown in Figure 2.

Our results for neutrino clustering can be compared with the Tremaine-Gunn bound [27], which gives an upper limit on the neutrino density in the core of a halo based on the argument that the maximum coarse grained phase space density can not exceed the maximum initial phase space density due to phase mixing. Their results are not directly applicable to our problem because in their derivation, neutrinos are assumed as the sole constituent of dark matter, and the coarse grained neutrino distribution is assumed to be Maxwell-Boltzmann instead of Fermi-Dirac for computational convenience. More recent work [34] has extended the derivation to models including both CDM and neutrinos and obtained $\rho_\nu \leq |2\Phi|^{3/2}m_\nu^4/12\pi^4$, where Φ is the gravitational potential of the system. For the NFW profile, we find

$$\delta_\nu(r; m_\nu, r_s, \bar{\delta}) \lesssim 80 \left(\frac{m_\nu}{\text{eV}} \right)^3 \left(\frac{r_s}{\text{Mpc}} \right)^3 \bar{\delta}^{3/2} \times \left[\frac{r_s}{r} \ln \left(\frac{r}{r_s} + 1 \right) \right]^{3/2}. \quad (17)$$

Here r_s and $\bar{\delta}$ are properties of the CDM halo given by equation (14). For 0.7 eV neutrinos, for example, this formula gives $\delta_\nu < 4600, 3.7 \times 10^4, 3.1 \times 10^5$, and 2.7×10^6 for $10^{12}, 10^{13}, 10^{14}$ and $10^{15}M_\odot$ halos, respectively, at the scale radius r_s . One can see that this constraint is satisfied for all neutrino overdensities in Figures 1 and 2.

IV. IMPLICATIONS FOR ULTRA HIGH ENERGY COSMIC RAYS

In this section we apply the neutrino clustering results from Sec III to the Z-burst model for UHECRs. No previous work on the Z-burst model has included realistic calculations for δ_ν . Instead, the value of δ_ν has been chosen based on certain observational constraints [23] or physical arguments [15, 19] and has differed greatly from $\delta_\nu \sim 1$ to 10^5 . In Ref. [23], the value of δ_ν is inferred from the CDM distribution in our local universe but the large smoothing scale ~ 20 Mpc assumed in the calculation results in $\delta_\nu \sim 1$. In contrast, our results from Sec III show that δ_ν can be $\gg 1$ in the inner ~ 1 Mpc of CDM halos. In Refs. [15, 19], δ_ν is approximated based on phase-space arguments similar to that of [27]. While this approach gives an upper bound on the neutrino clustering, the actual overdensity can be significantly less, as we have discussed in the previous paragraph. In addition, the neutrino clustering scale of ≈ 5 Mpc assumed in [19] is much larger than what we find in our calculations. Our method gives specific predictions for δ_ν as a function of halo radius, halo mass, and neutrino mass.

To estimate the cosmic ray flux we follow the standard assumption in the Z-burst model that the UHECRs above the GZK cutoff of 4×10^{19} eV are produced by the resonant $\nu\bar{\nu}$ scattering, while the lower energy events are explained by protons originating from a uniform distribution of extragalactic sources. The latter appears consistent with the isotropic distribution of $E < 4 \times 10^{19}$ eV events detected in AGASA and HiRes [35]. We compute the cosmic ray flux (in units of $(\text{eV m}^2 \text{ s sr})^{-1}$) from the Z-burst model with [23]

$$F_Z(E) = \int_0^\infty dE_p \int_0^{R_{max}} dr \left[\int_0^\infty dE_{\nu_i} F_{\nu_i}(E_{\nu_i}, r) n_{\bar{\nu}_i}(r) + \int_0^\infty dE_{\bar{\nu}_i} F_{\bar{\nu}_i}(E_{\bar{\nu}_i}, r) n_{\nu_i}(r) \right] \times \sigma_{\nu_i \bar{\nu}_i}(s) \text{Br}(Z \rightarrow \text{hadrons}) \frac{dN_{p+n}}{dE_p} \left| \frac{\partial P_p(r, E_p; E)}{\partial E} \right|. \quad (18)$$

Here $F_{\nu_i}(E_{\nu_i}, r)$ is the flux of ultra high energy neutrinos with energy E_{ν_i} at distance r and $n_{\nu_i}(r)$ is the physical number density of the relic neutrinos. (The repeated index i is summed over different neutrino species.)

The particle interactions are described by the cross section $\sigma_{\nu_i \bar{\nu}_i}(s)$ for the Z-boson production at the center-of-mass energy $s = 2m_\nu E_\nu$, and by the branching ratio $\text{Br}(Z \rightarrow \text{hadrons}) = 69.89 \pm 0.07 \%$ for the subsequent

cascade of the Z-boson into hadrons [36]. The factor dN_{p+n}/dE_p gives the energy distribution of the produced protons and neutrons. The subsequent proton propagation is specified by $P_p(r, E_p; E)$, which gives the probability that a proton created at distance r with energy E_p arrives at Earth with an energy greater than E . It measures the amount of proton energy degradation due to the resonant photoproduction of pions and other processes discussed in Sec I. Specific values of P_p has been calculated in [37] for the range of parameters considered in this paper.

A key feature of the Z-burst model is that the cross section $\sigma_{\nu_i \bar{\nu}_i}(s)$ for $\nu \bar{\nu} \rightarrow Z^0$ is enhanced by several orders of magnitude at the resonant energy in the rest frame of the relic neutrinos [17]

$$E_{\nu_i}^{res} = \frac{M_Z^2}{2m_{\nu_i}} = 4.2 \times 10^{21} \text{eV} \left(\frac{1 \text{eV}}{m_{\nu_i}} \right), \quad (19)$$

where M_Z is the mass of the Z boson. The flux in Equation (18) therefore depends only on the neutrino resonant energy and not on the shape of the incident high energy neutrino spectrum. Equation (18) can then be written as

$$\begin{aligned} \epsilon F_Z(E) = & B \int_0^\infty dE_p \int_0^{R_{max}} \frac{dr}{R_{max}} [1 + z(r)]^3 \\ & \times [1 + \delta_\nu(r)] \frac{4m_\nu}{M_Z^2} Q_p \left(y = \frac{4m_\nu E_p}{M_Z^2} \right) \\ & \times \left| \frac{\partial P_p(r, E_p; E)}{\partial E} \right|, \end{aligned} \quad (20)$$

where δ_ν is the neutrino overdensity, $z(r)$ is the redshift of the production site as a function of radial distance r , and $\epsilon \approx 8 \times 10^{16} \text{ m}^2 \text{ s sr}$ is the total exposure estimated from the highest energy events [23]. The function Q_p is the boosted momentum distribution from hadronic Z decays and can be calculated from experimental data [23]. It has a fairly broad peak at $y \approx 10^{-2}$ and falls off approximately as y^{-7} for $y \gtrsim 0.5$. The factor B is the normalization of the overall flux of high energy neutrinos, which remains a free parameter in this calculation since no successful astrophysical model yet exists to explain the production of $\gtrsim 10^{21} \text{ eV}$ neutrinos [38, 39, 40]. We set B to 445 here, which is the best fit value to the existing cosmic ray data assuming that the entire cosmic ray flux above $4 \times 10^{19} \text{ eV}$ is due to the Z-burst model for $m_\nu = 0.39 \text{ eV}$ [23]. We also do not attempt to model the effect of source evolution in our calculations since it is again an unknown quantity and is easy to incorporate once its nature is known.

We first present results for the cosmic ray spectrum $F(E)$ in the Z-burst model ignoring the spatial clustering in the neutrinos, i.e., we assume $\delta_\nu = 0$ and $\rho_\nu = \bar{\rho}_\nu$ in equation (20). This assumption underestimates the flux in the Z-burst model, but we include the results here for comparison since this is a common assumption made in several Z-burst calculations [15, 23, 40]. Figure 5 compares the resulting $E^3 F(E)$ for neutrino masses 0.07, 0.3,

0.4, 0.7, and 1.8 eV. It depends strongly on the neutrino mass, with a larger amplitude at high energies for smaller neutrino masses. This is because the momentum distribution Q_p of the decay particles peaks at a higher energy for smaller m_ν . For a given m_ν , $E^3 F(E)$ decreases rapidly at $E \gtrsim 10^{21} \text{ eV}$ because Q_p falls off as $\sim y^{-7}$ for $y \gtrsim 0.5$. The integration is carried out to a maximum distance of $R_{max} = 2000 \text{ Mpc}$, but our results are insensitive to this choice as long as R_{max} is sufficiently beyond the GZK zone of $\sim 50 \text{ Mpc}$.

For comparison, the dotted curve in Figure 5 shows the cosmic ray flux for protons originating from a uniform distribution of extragalactic sources. It is computed from

$$\begin{aligned} F_{EG}(E) = & \int_0^\infty dE_p \int_0^{R_{max}} \frac{dr}{R_{max}} [1 + z(r)]^3 \\ & \times F_p(E_p) \left| \frac{\partial P_p(r, E_p; E)}{\partial E} \right|, \end{aligned} \quad (21)$$

where the unknown proton energy spectrum $F_p(E_p)$ is typically assumed to be a power law: $F_p(E_p) = \epsilon^{-1} A E_p^{-\beta}$. The shape of F_{EG} depends on the injection spectrum F_p , but for definiteness, we have assumed $\beta = 2.4$ and $A = 5.98 \times 10^{31}$ (and an upper energy cutoff of $E_p = 10^{23}$), which are found to be the best fit values [23] to the existing cosmic ray data. The GZK cutoff is clearly seen at $\sim 4 \times 10^{19} \text{ eV}$ in the dotted curve. The flux rises beyond $\sim 4 \times 10^{20} \text{ eV}$ because the photoproduction of pions is a resonant process where the cross section peaks at $E_p \sim 2.3 \times 10^{20} \text{ eV}$ [1] and decreases at higher energies, allowing a larger fraction of protons to reach us.

The predictions for the UHECR spectrum change significantly when we incorporate the neutrino overdensity δ_ν computed in Sec. III. To make realistic estimates for our local universe, we consider five lines of sight towards five of the most massive nearby clusters: Virgo, Centaurus, Hydra, Perseus-Pisces, and Coma, where the highest overdensity of neutrinos are expected. The distance, mass, rough angular extent, and equatorial coordinates of each of the clusters are listed in Table 1 [41, 42]. The cluster masses are taken from <http://cfa-www.harvard.edu/~huchra/clusters>, where they are estimated from galaxy velocities and the virial theorem. We caution that these values have large error bars. For example, the mass of Virgo [43, 44, 45, 46], the nearest cluster, has been estimated to be $1.5 - 6 \times 10^{14} M_\odot$ based on X-ray emission measurements by ROSAT [43], to $1.5 \times 10^{15} M_\odot$ based on the relativistic Tolman-Bondi method [44]. The Tolman-Bondi model is based on analytic solutions to the Einstein field equations for spherically symmetric pressure free overdensities in a homogeneous universe [44, 47].

Figure 6 shows our predictions for the cosmic ray flux towards these five lines of sight for four different neutrino masses. Along each line of sight, high energy neutrinos from extragalactic sources are assumed to traverse a uniform sea of background neutrinos plus an overdensity

TABLE I: Parameters of five nearby Clusters.

Name	Distance(Mpc)	Mass(M_\odot)	Angular Radius($^\circ$)	RA(h min)	Dec($^\circ$ min)
Virgo	15	7.9×10^{14}	5	12 29.6	+11 49
Centaurus	43	1.3×10^{15}	1.5	12 46.1	-41 02
Hydra	53	4.6×10^{14}	2	10 34.5	-27 16
Perseus-Pisces	76	5.5×10^{15}	7	03 15.3	+41 20
Coma	99	1.7×10^{15}	2.5	12 57.4	+28 15

of background neutrinos centered at the location of the given cluster, where δ_ν is computed from equation (12) for the mass of the cluster. We also include in our calculation a local δ_ν for the Local Group of mass $4 \times 10^{12} M_\odot$ [48]. Although this mass is small, its proximity to us makes a non-negligible contribution to the UHECR flux. Our main conclusion from Figure 6 is that the flux of UHECRs in the Z-burst model should show significant anisotropy if $m_\nu \gtrsim 0.3$ eV, with the largest flux coming from the Virgo cluster. For $m_\nu \lesssim 0.1$ eV, on the other hand, neutrinos are too hot to cluster appreciably even around the largest clusters in the universe, and the UHECR flux in the Z-burst model is nearly isotropic.

V. CONCLUSION AND DISCUSSION

We have introduced and tested a method based on the collisionless Boltzmann equation to calculate the gravitational clustering of massive neutrinos in CDM halos for realistic cosmological models. This method is valid for currently favored models with $\Omega_{\text{cdm}} \gg \Omega_\nu$ in which the clustering of neutrinos is mostly determined by the existing CDM halos while the clustering of the CDM is little affected by the neutrinos. One can then obtain the neutrino phase space distribution by solving the collisionless Boltzmann equation in a background potential given by the universal profile of CDM halos from high resolution simulations. The resulting Boltzmann equation is linear in the neutrino density contrast and has tractable integral solutions that require negligible computational time in comparison with N-body simulations. This method has enabled us to obtain specific predictions for the neutrino overdensity as a function of halo radius, halo mass, and neutrino mass for a wide range of parameters.

Our calculation shows that neutrinos with masses $\gtrsim 0.3$ eV can cluster appreciably in CDM potential wells with masses $\gtrsim 10^{13} M_\odot$. The predicted neutrino overdensity increases with both the neutrino mass and the halo mass, ranging from $\delta_\nu \sim 10$ for 0.3 eV neutrinos in $\sim 10^{13} M_\odot$ halos to $\delta_\nu \sim 1500$ for 1.8 eV neutrinos in $\sim 10^{15} M_\odot$. Specific predictions are plotted in Figures 2 and 3. Neutrino clustering has a strong impact on the Z-burst model that has been proposed as a possible explanation for the UHECR events. The predicted UHECR spectrum shown in Figures 5 and 6 depends sensitively on

the neutrino mass and overdensity, showing distinct spectral features towards nearby galaxy clusters if $m_\nu \gtrsim 0.3$ eV.

To illustrate the effects of neutrino mass and overdensity on the UHECR spectrum, we have chosen to normalize the flux in Figures 5 and 6 with the same value (i.e. $B = 445$ in eq. (20)) instead of adjusting it by fitting individual spectrum to existing data. We have nonetheless included current data from the AGASA [3] and HiRes [6] experiments in Figures 5 and 6 for comparison. More events are needed to discriminate the different models and the directional dependence. The large increase in flux towards Virgo is an interesting signature of the Z-burst model for upcoming experiments such as Auger [49] and OWL [50] with angular resolution of $\sim 1^\circ$. Experimental limits on the anisotropy would in turn imply small neutrino inhomogeneities in the Z-burst model and can be used to place upper bounds on the neutrino mass.

The implication of the neutrino clustering results presented in this paper extends beyond the problem of the UHECR spectrum. For UHECR, upcoming experimental results may converge on a spectrum that is consistent with the GZK cutoff and would therefore not require models such as the Z-burst. It is also likely that the Z-burst model is not the correct explanation for the UHECR events. However, the neutrino-anti-neutrino resonance scattering process remains one of few ways to detect the relic neutrinos, as first suggested in [17]. This paper has addressed neutrino clustering, a major uncertainty in all studies concerning relic neutrinos.

Acknowledgments

We thank Ed Bertschinger, Tom Weiler, Jon Arons, Bhuvnesh Jain, and Nick Sarbu for useful discussions. C.-P. M. acknowledges support of an Alfred P. Sloan Foundation Fellowship, a Cottrell Scholars Award from the Research Corporation, and NASA grant NAG 5-12173. A portion of the work was carried out at the Aspen Center for Physics. This research has made use of the NASA/IPAC Extragalactic Database (NED) which is operated by the Jet Propulsion Laboratory, California Institute of Technology, under contract with the National Aeronautics and Space Administration and the Vizier catalogue access tool, CDS, Strasbourg, France.

-
- [1] K. Greisen, Phys. Rev. Lett. **16**,748 (1966); G.T. Zat'sepin and V.A. Kuz'min, J. Exp. Theor. Phys. Lett. **4**,78 (1966); R.J. Gould and G. Schreder, Phys. Rev. Lett. **16**,252 (1966).
- [2] M. Nagano and A. A. Watson, Rev. of Mod. Phys. **72**, 689, 2000; A. V. Olinto, Phys. Rep. **333**, 329 (2000); P. Bhattacharjee and G. Sigl, Phys. Rep. **327**, 109 (2000); and references therein.
- [3] M. Takeda *et al.* Phys. Rev. Lett. **81**,1163 (1998); updates at website <http://www-akeno.icrr.u-tokyo.ac.jp/AGASA>.
- [4] D.J. Bird *et al.* [Hires Collaboration], Phys. Rev. Lett. **71**,3401 (1993); Astrophys. J. **424**, 491 (1994); Astrophys. J. **441**,144 (1995).
- [5] M.A. Lawrence, R.J. Reid and A.A. Watson, J.Phys. G **17**,733 (1991); M. Ave, J.A. Hinton, R.A. Vazquez, A.A. Watson and E. Zas, Phys. Rev. Lett. **85**,2244 (2000).
- [6] The HiRes Collaboration, astro-ph/0208243; astro-ph/0208301
- [7] N.N. Efimov *et al.*, in *Proceedings of the Astrophysical Aspects of the Most Energetic Cosmic Rays* (World Scientific, Singapore, 1991).
- [8] M.S. Longair, High Energy Astrophysics, Vol. 2, (Cambridge University Press, London, 1994); D. Fargion, R.V. Konoplich and A. Salis, Z. Phys. C **74**,571 (1997); D. Fargion and A. Salis, Phys. Uspekhi **41**(8), 823.
- [9] J. Arons, submitted to Astrophys. J. (2002) and references therein.
- [10] D. Fargion and A. Salis, Nucl. Phys. Proc. Suppl. B **43**,269 (1995).
- [11] S. Fukuda *et al.* [Super-Kamiokande Collaboration], Phys. Rev. Lett. **86**, 5656 (2001) and references therein.
- [12] M. Ambrosio *et al.* [MACRO Collaboration], Phys. Lett. B **517**,59 (2001).
- [13] Q.R. Ahmad *et al.* [SNO Collaboration], Phys. Rev. Lett. **87**, 071301 (2001).
- [14] D. Fargion, B. Mele and A. Salis, Astrophys. J. **517**,725 (1999).
- [15] T. Weiler, Astropart. Phys. **11**,303 (1999).
- [16] G.M. Tanco, in *Physics and Astrophysics of Ultra-High-Energy Cosmic Rays*, ed. M. Lemoine and G. Sigl (Springer), 155 (2001).
- [17] T. Weiler, Phys. Rev. Lett. **49**,234 (1982).
- [18] E. Roulet, Phys. Rev. D **47**,5247 (1993).
- [19] S. Yoshida, G. Sigl and S. Lee, Phys. Rev. Lett. **81**,5505 (1998).
- [20] G. Gelmini and A. Kusenko, Phys. Rev. Lett. **82**,5202 (1999); Phys. Rev. Lett. **84**,1378 (2000).
- [21] J.L. Crooks, J.O. Dunn and P.H. Frampton, Astrophys. J. **546**,L1 (2001).
- [22] Z. Fodor, S.D. Katz and A. Ringwald, hep-ph/0105336.
- [23] Z. Fodor, S.D. Katz and A. Ringwald, J. High Energy Phys. **0206**,46 (2002).
- [24] J.F. Navarro, C.S. Frenk and S.D.M. White, Astrophys. J. **462**,563 (1996).
- [25] R. Brandenberger, N. Kaiser and N. Turok, Phys. Rev. D **36**,2242 (1987).
- [26] E. Bertschinger and P.N. Watts, Astrophys. J. **328**,23 (1988).
- [27] S. Tremaine and J.E. Gunn, Phys. Rev. Lett. **42**,407 (1979).
- [28] L. Kofman, A. Klypin, D. Pogosyan and J.P. Henry, Astrophys. J. **470**,102 (1996).
- [29] Ø. Elgarøy *et al.*, astro-ph/0204152.
- [30] J.S. Bullock *et al.*, Mon. Not. R. Astron. Soc. **321**,559 (2001).
- [31] C.-P. Ma and J.N. Fry, Astrophys. J. **543**,503 (2000).
- [32] S. Dodelson, E. Gates and A. Stebbins, Astrophys. J. **467**,10 (1996).
- [33] E.W. Kolb and M.S. Turner, The Early Universe, (Addison-Wesley Publishing Company,1990).
- [34] A. Kull, R.A. Trueman and H. Böhringer, Astrophys. J. **466**,L1 (1996).
- [35] V. Berezhinsky and A.A. Mikhailov, Phys. Lett. B **449**,237 (1999); G.A. Medina Tanco and A.A. Watson, Astropart. Phys. **12**,25 (1999); T. Weiler, hep-ph/0103023.
- [36] D.E. Groom *et al.* [Particle Data Group Collaboration], Eur. Phys. J. C **15**,1 (2000).
- [37] Z. Fodor and S.D. Katz, Phys. Rev. D **63**,023002 (2001).
- [38] A. Venkatesan, M.C. Miller and A.V. Olinto, Astrophys. J. **484**,323 (1997).
- [39] E. Waxman, astro-ph/9804023; E. Waxman and J. Bahcall, Phys. Rev. D **59**,023002 (1999); J. Bahcall and E. Waxman, Phys. Rev. D **64**,023002 (2001).
- [40] G. Gelmini and G. Varieschi, hep-ph/0201273.
- [41] F. Ochsenbein, P. Bauer and J. Marcout, Astron. Astrophys. Suppl. Ser. **143**,23 (2000).
- [42] NASA/IPAC Extragalactic Database.
- [43] H. Böhringer *et al.*, Nature **368**,828 (1994).
- [44] P. Fouqué, J.M. Solanes, T. Sanchis and C. Balkowski, Astron. and Astrophys. **375**,770 (2001).
- [45] R.B. Tully and E.J. Shaya, Astrophys. J. **281**,34 (1984); in *Evolution of Large Scale Structure*, ed. R.F. Stain and A.G.W. Cameron (ESO, Garching),333 (1998).
- [46] S. Schindler, B. Binggali and H. Böhringer, Astron. and Astrophys. **343**,420 (1999).
- [47] T. Ekholm *et al.*, Astron. and Astrophys. **351**, 827(1999).
- [48] I.M. Schmoldt and P. Saha, Astron. J. **115**,2231 (1998); D.M. Goldberg, Astrophys. J. **550**,87 (2001).
- [49] M. Kleifges *et al.* [Auger Collaboration], in *Proceedings of ICHEP 2000*, Osaka (World Scientific, 2000); Auger website <http://www.auger.org/>.
- [50] J.F. Krizmanic *et al.* [OWL/AirWatch Collaboration], in *Proceedings of the 26th International Cosmic Ray Conference*, Salt Lake City, 1999; OWL website <http://owl.gsfc.nasa.gov/intro.html>.

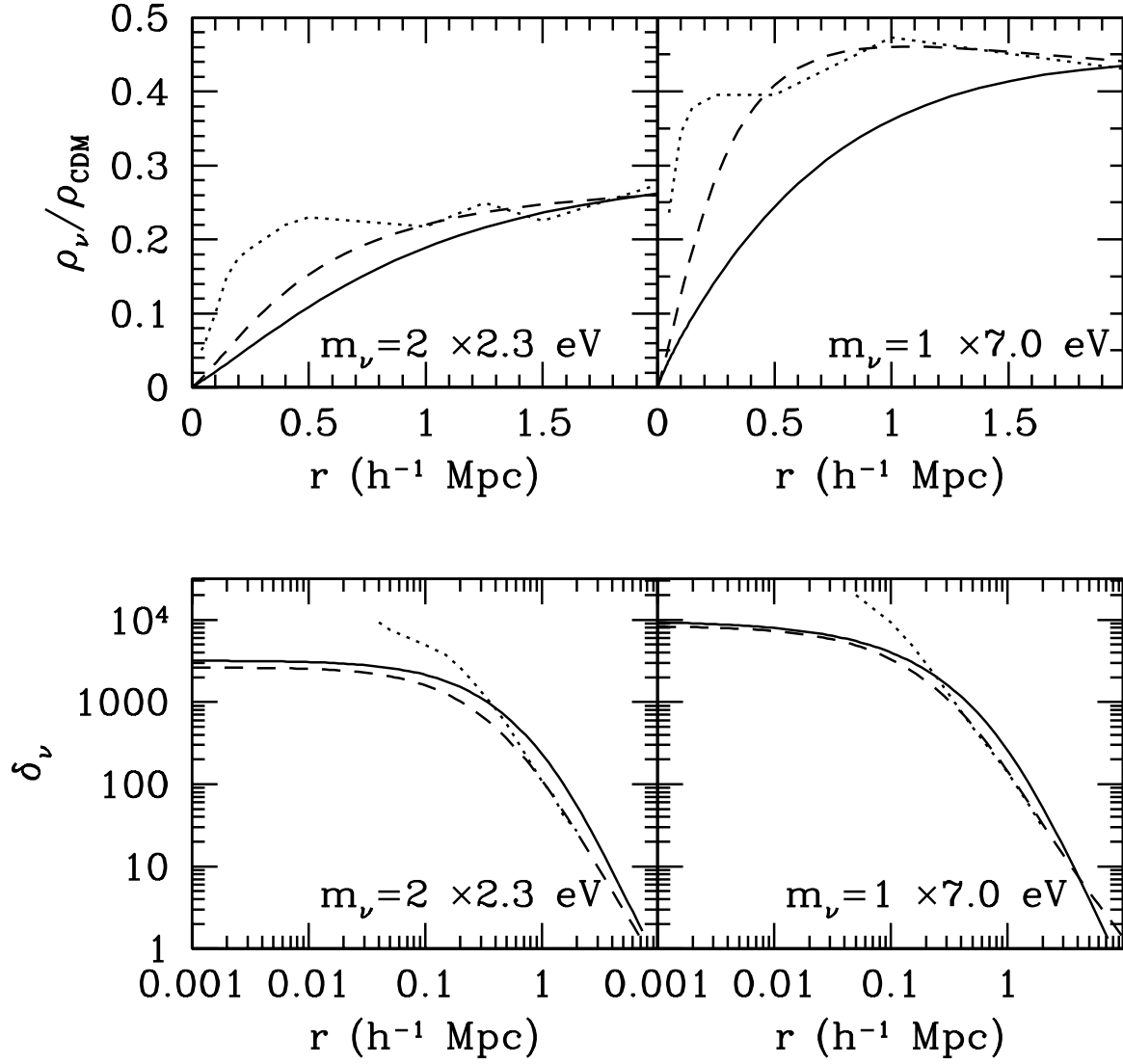


FIG. 1: Neutrino clustering calculated with our Boltzmann approach (dashed) vs. numerical simulations from [28] (dotted). The simulation resolution is $62.5 \text{ h}^{-1} \text{ kpc}$. The upper panels show the ratio of the neutrino density ρ_ν to the CDM density ρ_{CDM} as a function of radius for two halos of $1.3 \times 10^{15} M_\odot$ in two cosmological models. The lower panels show the neutrino overdensity $\delta_\nu = \rho_\nu/\bar{\rho}_\nu - 1$ for the same models. The solid curves compare neutrino clustering around CDM halos with an NFW profile [24] to illustrate how neutrinos respond to different gravitational potentials.

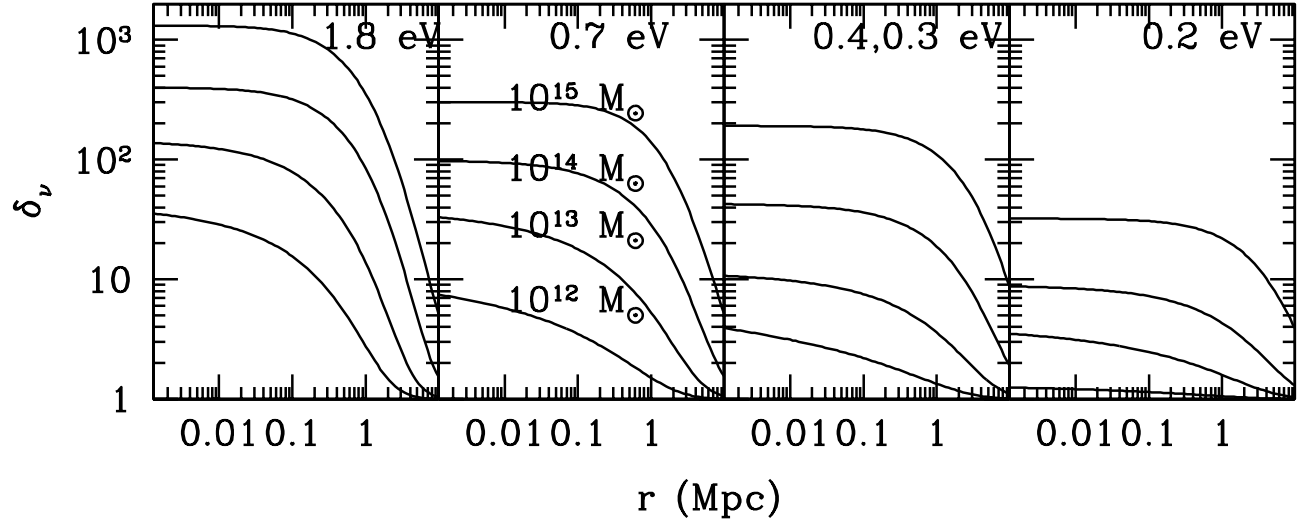


FIG. 2: Present-day neutrino overdensity δ_ν as a function of halo radius for different neutrino masses and halo masses. The clustering generally decreases as the neutrino mass is lowered (from left to right panels), a result of increasing neutrino thermal velocity and more effective free streaming. Within each panel, the curves show how δ_ν decreases as the halo mass is lowered from 10^{15} to $10^{12} M_\odot$, a result of shallower gravitational wells and smaller halo velocity dispersions compared with the neutrino thermal velocity. The similarity between the middle two panels indicates that neutrino clustering is more sensitive to the sum of the neutrino masses than how the mass is distributed among the three species. This figure shows that neutrinos with $m_\nu \gtrsim 0.2$ eV cluster appreciably in $M > 10^{12} M_\odot$ halos.

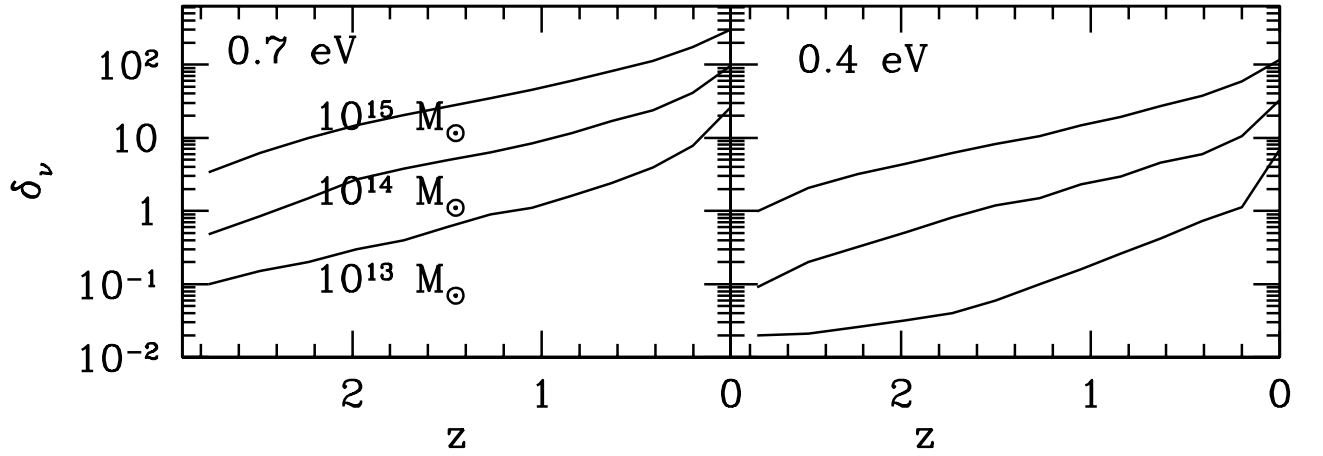


FIG. 3: Time evolution of the neutrino overdensity in the inner parts of the halos (where δ_ν is independent of radius) for $m_\nu = 0.7$ (left) and 0.4 eV (right). In each panel, three halo masses 10^{15} , 10^{14} , and $10^{13} M_\odot$ are shown (top down). Neutrinos start to cluster significantly only at late times, with $\gtrsim 75$ % of the clustering taking place between $z = 1$ and 0 .

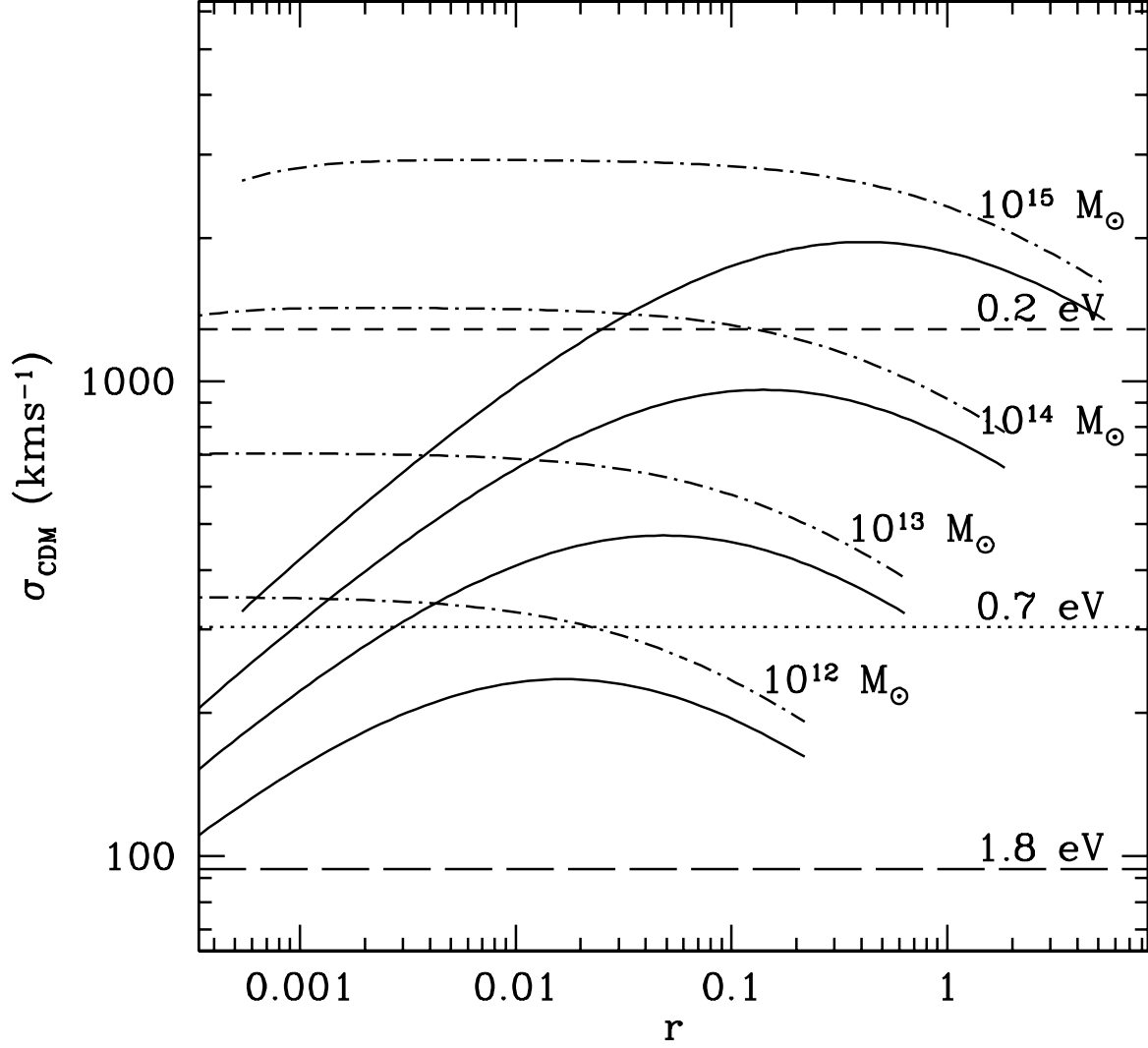


FIG. 4: Velocity dispersion of NFW halos of mass 10^{15} , 10^{14} , 10^{13} , and $10^{12} M_{\odot}$ (top down) as a function of halo radius. Two velocity orbits for the halo particles are shown for comparison: isotropic (solid) and $\beta \equiv 1 - v_t^2/v_r^2 = 0.5$ (dot-dashed). The horizontal lines indicate the present-day median thermal velocity for 0.2, 0.7, and 1.8 eV neutrinos. The values suggest that $m_{\nu} \gtrsim 0.2$ eV neutrinos are cold enough to cluster gravitationally, particularly in massive halos.

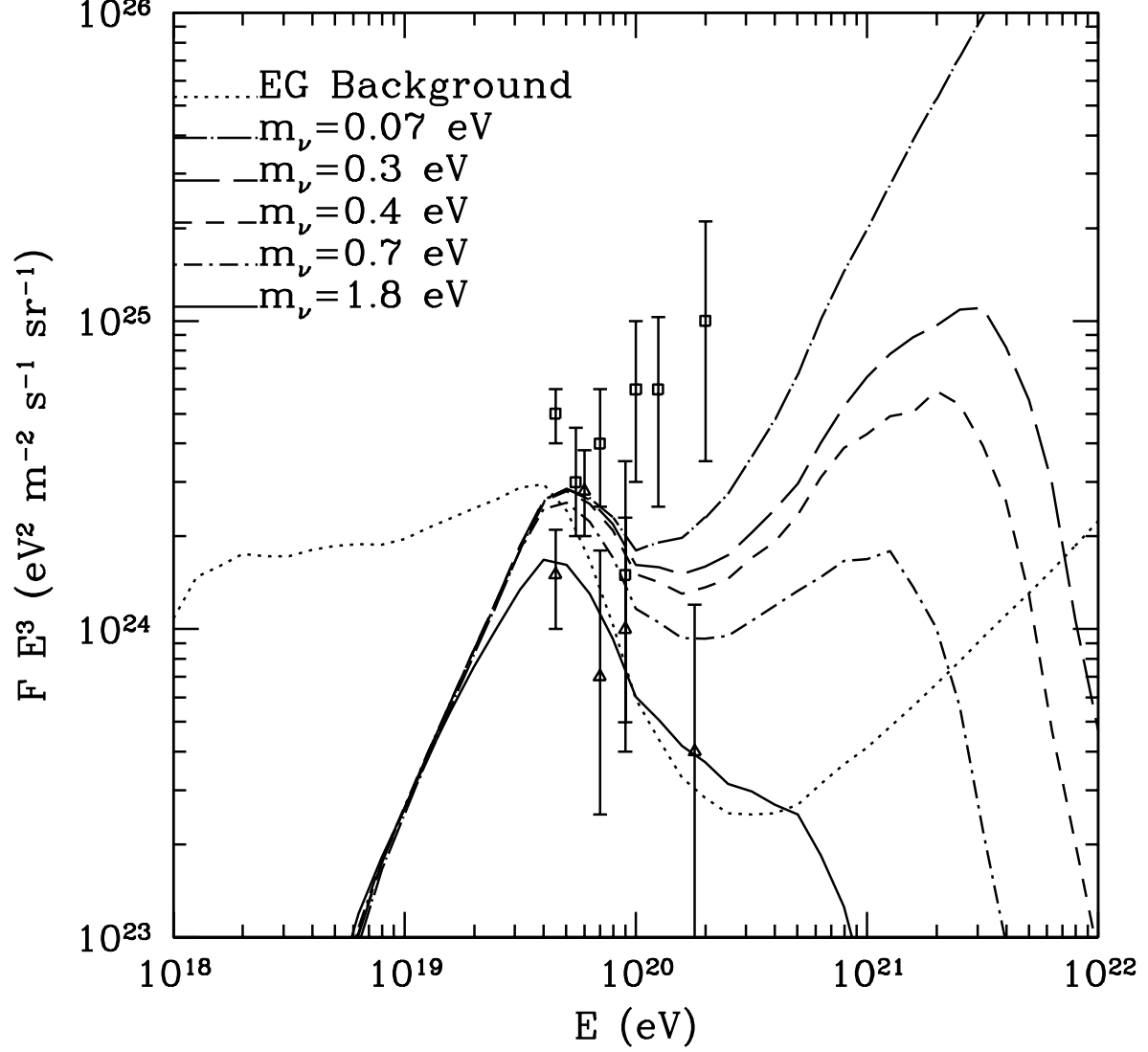


FIG. 5: Predictions for the cosmic ray flux produced in the Z-burst model when the relic neutrino density is assumed to be the big bang uniform background density without gravitational clustering. Five neutrino masses are shown: 1.8, 0.7, 0.4, 0.3, and 0.07 eV (from bottom up). The cosmic ray spectrum of protons originating from a uniform extragalactic background sources is shown for comparison (dotted). The GZK suppression in the flux is clearly seen at $E \gtrsim 4 \times 10^{19}$ eV in all spectra. The squares show the current 30 UHECR events from AGASA [3]; the triangles show the five HiRes events [6].

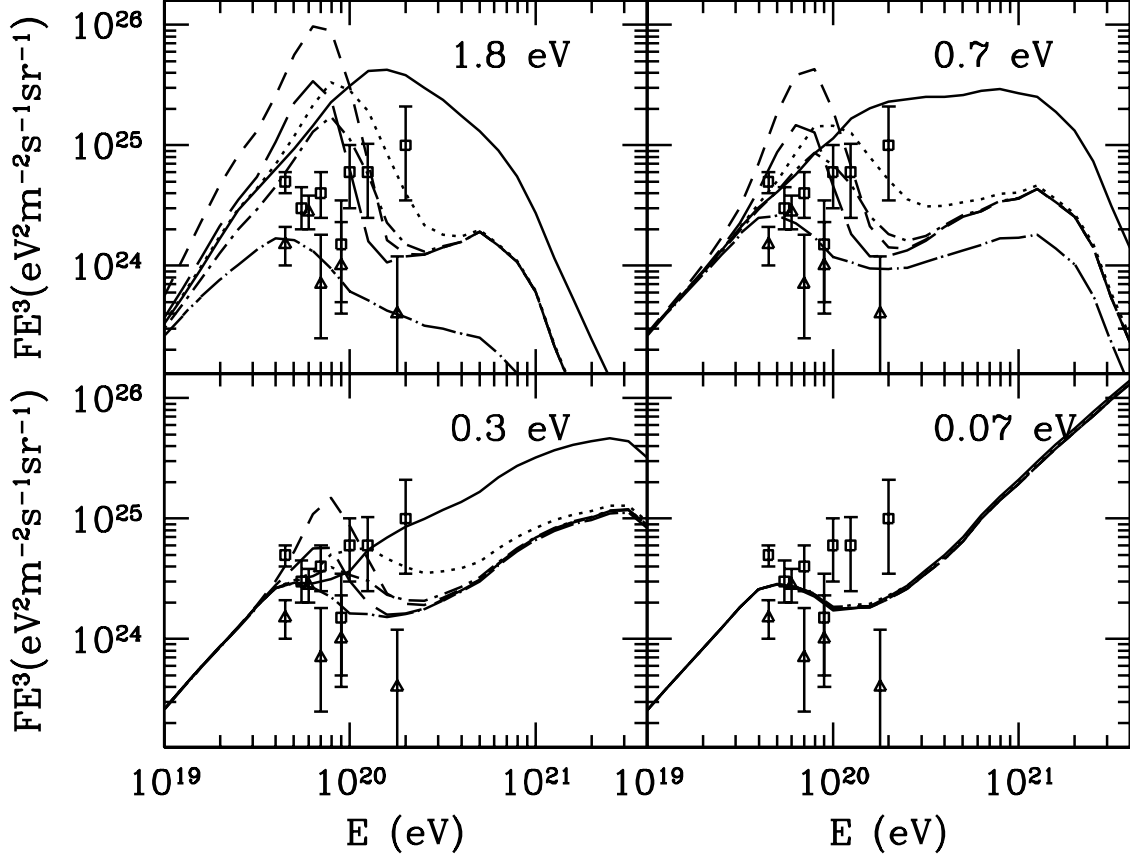


FIG. 6: Predictions for the cosmic ray flux produced in the Z-burst model using realistic neutrino overdensity computed in this paper. The four panels compare the UHECR spectrum for 4 different neutrino masses. Within each panel, our predictions for the spectrum towards five of the most massive clusters in the local universe are shown: Virgo (solid), Centaurus (dotted), Hydra (dot short-dashed), Perseus-Pisces (short dashed), and Coma (long dashed). For comparison, the dot-long-dashed curve shows the spectrum when neutrino clustering is ignored (i.e. the same as in Fig. 5). For $m_\nu \gtrsim 0.3$ eV, we predict that the Z-burst model should produce distinct spectrum towards each line of sight. For $m_\nu \lesssim 0.1$ eV, neutrino clustering is insignificant and the spectrum is expected to be nearly isotropic as seen in the lower right panel. The data points are the same as in Fig. 5.